Journal of Materials Chemistry A

Photo-Driven Growth of Monolayer of Platinum Spherical-Nanocrowns Uniformly Coating on Membrane toward Fuel Cell Applications

Journal:	*Journal of Materials Chemistry A*
Manuscript ID	TA-ART-07-2020-007189.R2
Article Type:	Paper
Date Submitted by the Author:	06-Oct-2020
Complete List of Authors:	Liu, Huiyuan; Dalian University of Technology, State Key Laboratory of Fine Chemicals; Dalian Institute of Chemical Physics Qin, Jiaqi; Dalian University of Technology, State Key Laboratory of Fine Chemicals, School of Chemical Engineering Rockward, Tommy ; Los Alamos National Laboratories Wu, Jingtian; University of California Irvine Department of Mechanical and Aerospace Engineering Li, Jia; Dalian University of Technology, School of Chemical Engineering Li, Guangwei; Sunrise Power CO., LTD Mao, Qing; Dalian University of Technology, College of Chemical Engineering Lv, Yang; Dalian University of Technology Wang, Xiao; ShanghaiTech University Zhang, Shuomeng ; Zhejiang University, College of Chemical & Biological Engineering Shi, Weiyu; Sunrise Power CO., LTD Chen, Gang; ShanghaiTech University, School of Physical Science and Technology He, Qinggang; Zhejiang University, College of Chemical & Biological Engineering Jiang, Yingbing; University of New Mexico, E & PS Yu, Hongmei; Dalian Institute of Chemical Physics, Chinese Academy of Sciences, Borup, Rodney; Los Alamos National Lab, Wang, Yun; The Univeristy of California, Irvine, Mechanical and Aerospace Engineering Song, Yujiang; Dalian University of Technology, c. State Key Laboratory of Fine Chemicals

ARTICLE

Photo-Driven Growth of Monolayer of Platinum Spherical-Nanocrowns Uniformly Coating on Membrane toward Fuel Cell Applications

Received 00th January 20xx,
Accepted 00th January 20xx

DOI: 10.1039/x0xx00000x

Huiyuan Liu[a,b] , Jiaqi Qin[a], Tommy Rockward[c], Jingtian Wu[d], Jia Li[a], Guangwei Li[e], Qing Mao[a], Yang Lv[a], Xiao Wang[f], Shuomeng Zhang[g], Weiyu Shi[e], Gang Chen[f], Qinggang He[g], Ying-Bing Jiang[h], Hongmei Yu[b], Rodney L. Borup[c], Yun Wang[d]*, and Yujiang Song[a]*

Membrane electrode assemblies (MEAs) serve as the core units of polymer electrolyte membrane fuel cells (PEMFCs) and are regularly fabricated by painting a slurry of commercial Pt/C onto membrane, leading to thick and disordered electrocatalyst layers (CLs). Herein, we report a photo-driven fabrication of MEAs with ultra-thin and ordered CLs by growing monolayer of dendritic platinum spherical-nanocrowns onto each side of photocatalyst-modified membrane. This approach allows us to control the thickness and platinum loading of ordered CLs by simply varying the concentration of platinum precursor under tungsten light irradiation. The resultant MEAs exhibit an excellent fuel cell power density of 1.01 ± 0.05 W/cm^2 at a platinum loading of 53 ± 1.5 μg/cm$^2_{cathode}$. The exceptional activity is likely arising from nanostructured platinum crowns, efficient mass transport, and uniform reaction rate in the ultrathin (59 ± 12 nm thick) and ordered CLs according to electrochemical and theoretical investigations.

Introduction

Fuel cell vehicles poise a great potential to revolutionize today's automobile industry owning to environmental benignity and energy efficiency [1-4]. At the centre of PEMFCs resides MEAs that are generally fabricated by spraying a slurry of water, alcohol, ionomer, and commercial Pt/C onto each side of membrane, resulting in micron-scale thick and disordered CLs [5-7]. Such CLs frequently confront the challenge of inefficient mass transport of proton, electron, water, and gas together with non-uniformity of oxygen reduction reaction (ORR) [6-8]. In this regard, tremendous efforts have been contributed to the fabrication of MEAs with ordered CLs [7, 9-12].

Middelman *et al.* [9] first sketched an ordered CL, which is composed of vertically aligned electronic conductor loaded with platinum nanoparticles as a whole covered by 10 nm thick ionomer. Currently, ordered CLs can be categorized into four types, including ordered electronic conductors [11, 13, 14], ordered electrocatalysts [5, 7, 15, 16], ordered ionomer [17], and ordered non-conductive supports[18]. Especially, Debe and his co-workers pioneered the fabrication of nanostructured thin film (NSTF) CLs by sputtering platinum or platinum alloy onto oriented organic whiskers arrays [19]. The ordered CLs are advantageous for mass transport and ORR uniformity and allow researchers to realize a low platinum loading of 0.07-0.15 mg$_{Pt}$/cm$^2_{MEA}$ [11, 19, 20]. However, the fabrication methods of ordered CLs are still rare and most of previous ordered CLs are susceptible to topple over, thus losing structural order during decal or hot-pressing process [5, 19].

Herein, we report the photo-driven fabrication of ordered CLs comprised of monolayer of dendritic platinum spherical-nanocrowns completely and uniformly coating on photocatalyst-modified membrane. We investigated the photocatalytic nucleation and growth mechanism and realized control over the thickness and the platinum loading of ordered CLs. In particular, the resultant ordered CL with an average thickness of 59 ± 12 nm and a platinum loading of 53.3 ± 1.5 μg$_{Pt}$ /cm$^2_{cathode}$ survives hot-pressing process and reaches a maximum single cell power density of 1.01 ± 0.05 W/cm^2. The remarkable activity seems to originate from nanostructured platinum spherical-crown, efficient mass transport, and uniform ORR rate in the ultra-thin ordered CLs.

Experimental

Chemicals and Materials

[a] State Key Laboratory of Fine Chemicals, School of Chemical Engineering, Dalian University of Technology, Dalian, Liaoning 116024, China. Email: yjsong@dlut.edu.cn
[b] Dalian National Laboratories for Clean Energy, Dalian Institute of Chemical Physics, Chinese Academy of Sciences, Dalian, Liaoning 116023, China.
[c] Los Alamos National Laboratories, Los Alamos, NM 87545, USA.
[d] Mechanical & Aerospace Engineering, University of California, Irvine, CA 92697, USA. Email: yunw@uci.edu
[e] National Engineering Research Centre of Fuel Cell & Hydrogen Technology, Sunrise Power CO., LTD., Dalian, Liaoning 116024, China.
[f] School of Physical Science and Technology, ShanghaiTech University, Shanghai 201210, China.
[g] College of Chemical & Biological Engineering, Zhejiang University, Hangzhou, Zhejiang, 310058, China.
[h] Department of Earth and Planetary Sciences, University of New Mexico, NM 87131, USA.
Electronic Supplementary Information (ESI) available. See DOI: 10.1039/x0xx00000x

Potassium tetrachloroplatinate(II) (K_2PtCl_4, 46.48 wt.% Pt, Tianjin Fengchuan, China), Pluronic P123 ($PEO_{20}PPO_{70}PEO_{20}$, ethylene oxide-EO, propylene oxide-PO, Mn = 5800 g/mol, Sigma-Aldrich, USA) and L-ascorbic acid (AA, ≥ 99%, Sigma-Aldrich, USA) were of the highest purity available and were used as received. 30 wt% H_2O_2 and concentrated H_2SO_4 are analytical reagents and purchased from Kermel (Tianjin, China). Zn(II) meso-tetra(N-methyl-4-pyridyl)porphine tetratosylate (ZnP) photocatalyst and Zn(II) meso-tetra(4-sulfonatophenyl)porphine tetrasodium salt ($ZnTPPS_4$) was obtained from Frontier Scientific (USA) and used without further purification. Poly(perfluorosulfonic acid) (PFSA) NR212 membrane (~50 μm, unreinforced membrane), PFSA NR211 membrane (~25 μm, unreinforced membrane) and PFSA resin solution (5 wt% in the mixture of lower aliphatic alcohols and water, contains 45 wt% water) were obtained from DuPont and gas diffusion layer (GDL) was obtained from Sunrise Power CO., LTD. All aqueous solutions were prepared with ultrapure water (18.2 MΩ·cm at 25 °C) from a Millipore Nanopure water system (Synergy® UV, France).

Photo-driven Fabrication of Ordered CLs

Colorless PFSA membrane was immersed in 3 wt% of H_2O_2 aq. at 80 °C for 1 h and rinsed with boiling water to remove impurities, and then incubated in 0.5 M of H_2SO_4 aq. at 80 °C for 1 h and purified with boiling water.

A piece of purified PFSA membrane (4 cm * 4 cm) was initially submerged in 15 mL of 100 μM ZnP aq. at 25 °C for 12 min to allow ZnP molecules to self-assemble into the matrix of PFSA membrane. Next, the ZnP photocatalyst-decorated greenish PFSA membrane was vertically fixed in the middle of a bi-square-windowed (2 cm * 2 cm) demountable reactor to form two separated liquid-tight compartments, each with a volume of 0.74 mL. Next, the two sides of the ZnP-decorated PFSA membrane were simultaneously irradiated with tungsten light (515 nmoles·cm^{-2}·s^{-1}) in the presence of freshly prepared 1.0-2.2 mM of K_2PtCl_4 aq., 50 mM AA aq. as the electron donor, and 0.067 mM of Pluronic P123 aq. as the capping agent. To mitigate the heating effect by irradiation, the reactor was placed in an ice-water bath to control the temperature during irradiation. After 1.5-4 min of irradiation, both sides of the membrane became black. Because the black platinum nucleation centers block the light source, the photocatalytic process was shut down automatically. In the following, the chemical autocatalytic reduction of platinum complexes on pre-formed platinum nucleation centers was continued for at least 7 h for completion under room light (0.18 nmoles·cm^{-2}·s^{-1}) to form mirror-like black platinum coatings. The light intensity was measured with a Digital Light Meter (TES-1339, Taipei, China).

Lastly, the platinum-coated membrane was incubated in 3 wt.% of H_2O_2 aq. at 80 °C for 1 h and subsequently in 0.5 M of H_2SO_4 aq. at 80 °C for 1 h as well as washed with copious amount of boiling water to remove as many impurities and by-products as possible, and air-dried on a vacuum hot-plate for future use.

Assembly of PEMFCs and Electrochemical Evaluation

The geometric area of a typical MEA coated with ordered CLs is about 2.89 cm^2 due to water loss and shrinkage. A MEA was hot-pressed in-between GDL at 125 °C under 6.4 MPa for 2 min. For comparison, conventional MEAs were also prepared by successively spraying a slurry (1 $mg_{Pt/C}$/mL) of water, ethanol, PFSA resin solution (v:v:v=1:9:0.065), and commercial Pt/C (70 wt.%, Johnson Matthey) onto each side of a PFSA NR211 membrane on a vacuum hot-plate at 70 °C to reach 0.1 mg_{Pt}/cm^2 for both anodic and cathodic platinum loading. The conventional MEA was hot-pressed in-between GDL at 130 °C under 6.4 MPa for 2 min.

Each MEA was placed into a single-cell unit, equipped with graphite bipolar plates with a serpentine gas flow channel. Single cell performance was evaluated on a house-made fuel cell test station at a cell temperature of 90 °C. The anode and cathode were fed with humidified H_2 and O_2 with a flow rate of 100 mL/min and 200 mL/min, respectively. The back pressure for both the anode and the cathode were 0.2 MPa_{gauge}. An Impedance Meter (PLZ 664WA, Kikusui, Japan) was employed to record I-V curves.

Electrochemical impedance spectroscopy (EIS) was carried out to investigate MEAs at 0.8 V (vs. RHE) by applying an AC amplitude of 10 mV over the AC frequency range from 20 kHz to 100 Hz on an Autolab potentiostat/galvanostat (Echo Chemie BV Model PGSTAT-302N, Netherlands).

Cyclic voltammetry (CV) curves were collected on an electrochemical analyzer (CHI 760D, Chenhua Instruments, China) to investigate electrochemically active surface area (ECSA) at 30 °C with a sweep rate of 50 mV/s. The ECSA values were estimated by measuring the charges associated with H_{upd} desorption (Q) between 0.1 and 0.4 V after double-layer correction and assuming a value of 210 μC/cm^2 for the desorption of a monolayer of hydrogen onto platinum surface (q_H). The ECSA values were calculated based on the following equation:

$$ECSA = Q/(mq_H) \quad (1)$$

where Q is the charge associated with H_{upd} desorption, m is the mass of loaded metal, and q_H is the charge required for the desorption of a monolayer of hydrogen on Pt surface.

Physical characterizations

UV-visible spectra were obtained with a spectrophotometer (Analytic Jena, Specord S600) and a 0.2 cm path length quartz cell. The UV-visible spectra of PFSA membrane with and without ZnP were carried out by vertically fixing the membrane in the light path. Fourier transform infrared spectra (FT-IR, Nicolet 6700 spectrometer) were recorded at a resolution of 4 cm^{-1}.

The morphologies of CLs were investigated by scanning electron microscope (SEM, 1-3 keV S-5200 & S-5800). To view the cross-section images, the MEAs coated with ordered CLs were frozen in liquid nitrogen for at least 15 min, and then broken off by slightly pressing. The fragments of the MEAs coated with ordered CLs were adhered to a sample stage with conductive adhesive.

Transmission electron microscope (TEM) and high-angle annular dark-field (HAADF) TEM were carried out on FEI Tecnai F30 operated at 300 keV. The samples for the TEM analysis were prepared by adding drops of colloidal solution onto a holey carbon-coated copper grid. The grids were further dried in air prior to imaging.

To measure the platinum loading, the MEAs coated with ordered CLs were immersed in aqua regia solution ($HCl:HNO_3$ = 3:1). Next, the mixture was diluted for the analysis of platinum content with ICP-OES (Perkin Elmer ICP-OES Optima2000DV). Current sensing atomic force microscope (CSAFM) analysis was carried out on Agilent AFM 5500. CSAFM current images of PFSA NR212 and ZnP-modified PFSA NR212 were taken at 25 ^oC, RH 87%, and a bias of -2 V. The X-ray diffraction (XRD) patterns of single-side platinum coated membranes were collected on a Rigaku Smartlab powder diffractometer with a Cu Kα radiation source (45 kV, λ = 0.15432 nm) at a scanning rate of 5°/min.

Results and discussion

Photo-driven Fabrication of Ordered CLs

Briefly, a sheet of hydrated colorless membrane is incubated in ZnP (Fig. 1a, 1b) aq. to allow ZnP molecules to self-assemble into the matrix of membrane. This self-assembly process is driven by electrostatic interaction between positively charged ZnP and negatively charged sulfonic groups of membrane, which cannot be accomplished by using negatively charged porphyrin (Fig. S1). After the self-assembly, the ZnP photocatalyst-modified membrane turns to be greenish (Fig. 1c) and the ZnP exists as single molecules as evidenced by UV-vis and FT-IR (Fig. 1d-e and Fig. S2). The loading of ZnP is 20.2 ± 0.2 $\mu g/cm^2$ according to UV-vis measurements (Fig. S3). The incorporation of ZnP in membrane has negligible influence on the membrane proton conductivity based on through-plane proton conductivity assessment by CSAFM (Fig. 1f-g) and the chemical durability of the membrane in the Fenton reagent (Fig. S4). This is consistent with the almost identical single cell performance by using either pristine membrane or ZnP-modified membrane to fabricate MEAs and to carry out single cell tests (Fig. S5).

The ZnP-modified membrane is vertically fixed in the middle of a demountable reactor to form two separated liquid-tight reaction compartments. Next, the two sides of the ZnP-modified membrane are simultaneously irradiated with double tungsten light in the presence of freshly prepared K_2PtCl_4 aq., ascorbic acid (AA) aq., and P123 (Fig. 1h). After irradiation, each side of the whole area of the ZnP-modified membrane in contact with the reaction mixture turns black. See more details in the Materials and Methods.

Under tungsten light irradiation, photocatalytic nucleation occurs at the interface of reaction mixture/membrane as depicted in Fig. 1i [21]. Absorption of visible light by ZnP yields a long-lived excited triplet π-π* state, ZnP*, which is a strong reducing agent ($ZnP^*/ZnP^{\cdot+}$, –0.75 V) [22, 23] capable of rapidly reducing Pt^{2+} to zero-valent platinum atoms. Meanwhile, ZnP* is oxidized to form $ZnP^{\cdot+}$. In the following, $ZnP^{\cdot+}$ is reduced by electron donor (AA) to regenerate neutral ZnP, which can absorb light and initiate another photocatalytic cycle. After a number of cycles, platinum nucleation centres are formed in the vicinity of ZnP. This interfacial photocatalytic nucleation enables platinum to regio-selectively grow on both sides of the membrane instead of in the reaction mixture. When the membrane turns black, the light cannot reach ZnP anymore and the photocatalytic nucleation is terminated. Next, platinum nucleation centres autocatalytically grow into larger nanostructures under room light to form mirror-like CLs (Fig. 1j and 1k).

Structure, Formation Mechanism, and Control of CLs

SEM reveals that when a single-side metal loading is 37.2 ± 1.9 $\mu g_{Pt}/cm^2$ as determined by ICP-OES (Table S1), spherical nanostructures with an average top-view diameter of 87 ± 22 nm are obtained and partially coat the membrane as a sub-monolayer (Fig. 2a-b and Fig. S6). Interestingly, cross-section view of liquid nitrogen cryo-brittle-fractured platinum sub-monolayer shows that the nanostructures virtually take a novel spherical-crown shape like a wetting droplet spreading on membrane, corresponding to a sub-monolayer thickness of 47 ± 8 nm (Fig. 2c and Fig. S6). This relatively large contact area suggests that the platinum spherical-nanocrowns may strongly adhere to membrane and would not be easily detached. Actually, no visible detachment of the spherical-crowns from membrane is observed within 10 min of sonication in a water-bath cleaner. TEM and HAADF-TEM images show that the spherical-crowns are dendritic with typical 2-3 nm branches in diameter (Fig. 2d-f). High-resolution TEM image and selected-area electron diffraction (SAED) (Fig. 2f) show that the spherical-crowns are face-centred cubic (fcc) polycrystalline structures.

To gain more insights into the regio-selectively photocatalytic nucleation and autocatalytic growth process, SEM samples were sequentially prepared at specific times during 150 s of irradiation by washing with copious amount of water and air-drying to effectively interrupt the reaction and thus catching a snapshot of the reaction. This time-development study reveals the structural evolution of the sub-monolayer of dendritic platinum spherical-nanocrowns as shown in Fig. S7. After 90 s of illumination, platinum nucleation centers begin forming, but there are only a few. After 100 s of illumination, many platinum nucleation centers are formed. Next, new platinum nucleation centers are continuously formed throughout the illumination process. The number density of platinum seeds increases from 84 ± 4 /μm^2 at 100 s to 334 ± 3 /μm^2 at 150 s (Fig. 3) and so does the top-view diameter of the nascent platinum spherical-nanocrowns during the illumination period (Fig. 3, Fig. S7-8).

Based on the elucidation on the formation mechanism, the platinum loading on the membrane has been readily tuned by varying the concentration of K_2PtCl_4 aq. under irradiation. As the single-side loading increases to be 53.3 ± 1.5 $\mu g_{Pt}/cm^2$, dendritic spherical-crowns possess an average top-view diameter of 83 ± 16 nm. The dendritic spherical-crowns form an uniform monolayer with rich voids and fold belts at an average

thickness of 59 ± 12 nm (Fig. 4a-c and Fig. S9). At a loading of 70.1 ± 3.0 and 83.1 ± 1.1 $\mu g_{Pt}/cm^2$, the average top-view diameter of spherical-crowns becomes 76 ± 19 and 87 ± 20 nm, respectively, and the monolayer thickness turns to be 68 ± 6 and 76 ± 8 nm, respectively (Fig. 4d-i, Fig. S10-11). In the latter two cases, the dendritic spherical-crowns tend to pack together more tightly with less voids and even larger fold belts. It is certain that the dehydration of the coated membrane has led to lateral shrinkage[24] and consequently "mountain genesis" occurs in the CL (Fig. 4j), in good agreement with the loss of shiny metal lustre after the coated membrane being dried. XRD patterns of the single-side coated membrane with different platinum loadings display characteristic diffraction peaks of fcc platinum (Fig. 4k).

It is worth pointing out that this photo-driven approach allows us to simultaneously grow platinum (sub)monolayer on both sides of the ZnP-modified membrane to bottom-up construct ordered CLs unlike traditional microemulsion-up fabrication process requiring two separate painting processes. Fig. 5a-c shows the cross-section view of a MEA with two integrated ordered CLs fully and homogeneously coating on the sandwiched membrane. The thickness of the platinum (sub)monolayer has been manipulated to be less than 100 nm. The ultra-thin and ordered CLs are expected to provide shortened and non-tortuous transport route good for mass transport, which agrees well with previous study on 3M's NSTF CLs [25].

Electrochemical Performance and Theoretical Evaluation

A purified MEA with two ultra-thin ordered CL was hot-pressed in-between two gas diffusion layers. Interestingly, the CLs well survived the hot-pressing process due to the robustness of constituent dendritic platinum spherical-nanocrowns, different from other types of ordered CLs prone to toppling over while being hot-pressed[5, 19] (Fig. 5d-f).

We investigated the effect of cathodic platinum loading on single cell performance while holding anodic platinum loading of 37.2 ± 1.9 $\mu g_{Pt}/cm^2_{anode}$ constant as shown in Fig. 6a and 6b. The peak power density of single cells reaches 0.526 ± 0.020, 0.822 ± 0.066, 0.830 ± 0.032 and 0.812 ± 0.028 W/cm² at 37.2 ± 1.9, 53.3 ± 1.5, 70.1 ± 3.0 and 83.1 ± 1.1 $\mu g_{Pt}/cm^2_{cathode}$, corresponding to mass specific power densities of 7.11 ± 0.27, 9.13 ± 0.73, 7.74 ± 0.3 and 6.77 ± 0.23 $W/mg_{Pt\ total}$ and cathode mass specific power densities of 14.22 ± 0.54, 15.51 ± 1.25, 11.84 ± 0.45 and 9.78 ± 0.34 W/mg_{Pt}, respectively. Overall, the cathodic loading of 53.3 ± 1.5 $\mu g_{Pt}/cm^2_{cathode}$ exhibits the highest activity.

To further optimize the single cell performance, the anodic humidifier temperature was tuned up from 90 to 95 °C, a little higher than the cell operation temperature of 90 °C. The single cell peak power density surges to be 1.01 ± 0.050 W/cm² (95 °C) from 0.822 ± 0.066 W/cm² (90 °C) (Fig. 6c), corresponding to a mass specific power density of 11.16 ± 0.55 $W/mg_{Pt\ total}$ and a cathodic mass specific power density of 18.89 ± 0.94 $W/mg_{Pt\ cathode}$(Fig. 6d). In this case, the activity enhancement likely arises from sufficient water available for proton transport in the ultra-thin ordered anodic CL, similar to 3M's NSTF CLs [26] and consistent with the electrochemical impedance spectroscopy results (Fig. S12 and Table S2). The peak mass power density of the ultra-thin ordered CLs is 1.4 times of the conventional disordered CLs (8.51 $W/mg_{Pt\ total}$) (Fig. S13). The mass specific power density of the ultra-thin ordered CLs is one of the highest among those reported in the literature (Table S3 and Fig. 7a). The single cell performance of the ultra-thin ordered CLs with an active geometrical area of 5 cm² was also evaluated at Los Alamos National Laboratory (Department of Energy, US), corroborating our results and exhibiting a reasonably good Tafel plot (Fig. S14). In addition, the performance of single cell equipped with the MEA with ultrathin ordered CL was also tested in H_2/air as shown in Fig. S15. The maximum power density is 0.435 W/cm².

To understand the origin of the high activity, we collected cyclic voltammogram (CV) curves (Fig. S16) of the ultra-thin ordered CLs as cathodes and determined ECSA values by measuring the charges associated with H_{upd} desorption (Q) between 0.1 and 0.4 V (vs. RHE) after double-layer correction and assuming a value of 210 μC/cm² for the desorption of monolayer hydrogen onto Pt surface (q_H). The ECSA value of the ultra-thin ordered CL is 5.1 ± 0.37 m²/g at platinum loading of 53.3 ± 1.5 $\mu g_{Pt}/cm^2$, quite similar to 5.35 ± 0.15, 5.68 ± 0.43 and 5.63 ± 0.84 m²/g at platinum loading of 37.2, 70.1 and 83.1 $\mu g_{Pt}/cm^2$, respectively. In addition, the ECSA of a conventional disordered CL is 30.3 m^2/g_{Pt} (Fig. S13), much higher than that of the ultra-thin ordered CL. This suggests that the ECSA should not be the only reason for the observed high activity. Furthermore, the ECSA value of the cathode with a Pt loading of 53.3 ± 1.5 $\mu g_{Pt}/cm^2$ is close to the outer surface area of solid Pt spherical-crown without dendritic features (~ $2.85_{spherical\ surface}$ + $0.94_{base\ plane}$ m^2/g_{Pt}). In other words, the interior of the dendritic spherical-crowns is not much accessible because of tiny and/or somehow blocked pores.

We then investigated ohmic polarization region around 0.55 V of the ultra-thin ordered CL with a platinum loading of 53.3 ± 1.5 $\mu g_{Pt}/cm^2$, which appears to be much better than those with other platinum loadings in terms of current density as shown in Fig. 6a [5, 27]. We speculate that the improved ohmic polarization may be due to the existence of rich voids and nano-crevices among the cracking platinum monolayer suitable for water management, consistent with previous study on the effect of nanocracks on water management [28].

To further understand the high activity of the ultra-thin ordered CLs, theoretical formula were employed to analyze ORR in the CLs. The oxygen transport loss across a CL can be expressed by equation (2) as follows [29].

$$\Delta C_{CL}^{O_2} \approx \frac{I\ \delta_{CL}}{4F D_{eff}^{O_2}} \qquad (2)$$

where $\Delta C_{CL}^{O_2}$ is oxygen transport loss, I is current density, F is Faraday constant (96485 C/mol), δ_{CL} is the thickness of CL, and $D_{eff}^{O_2}$ is diffusion coefficient of O_2 in CL (10^{-6} m²/s) [30, 31].

The variation of ORR rate j across a CL can be expressed by equation (3) and (4) as follows [31].

$$\frac{\Delta j \delta_{CL}}{I} = \frac{\Delta U}{2\frac{RT}{\alpha F}} \quad (3)$$

$$\Delta U = \frac{I\delta_{CL}}{\sigma_m^{eff}} \quad (4)$$

where $\frac{j\delta_{CL}}{I}$ is dimensionless reaction rate, R is the universal gas constant, T is the temperature of single cells (90 °C), α is the transfer coefficient, and σ_m^{eff} is the effective ionic conductivity.

The ultra-thin CLs can effectively minimize the oxygen transport loss (e.g. $\Delta C_{CL}^{O_2}$ <0.001 mol/m³ for 50 nm thick CL at 1 A/cm²) and thus well controlling the variation of ORR rate j across a CL. Fig. 7b-c present the spatial variation of the dimensionless reaction rate ($\frac{j\delta_{CL}}{I}$) across a CL at 1 A/cm² and 2.4 A/cm², respectively. The 50 nm thick CL has a reaction rate variation less than 0.5% in comparison with 87% for a 10 μm thick CL at 1 A/cm², and a reaction rate variation less than 1% versus 42% for a 2 μm thick CL at 2.4 A/cm². The 80 nm thick CL also has a low reaction rate variation (less than 2%) at 2.4 A/cm². Consequently, the ORR rate across the 59 nm thick CL in our case should be highly uniform and well contribute to the high activity.

Conclusions

In summary, ultra-thin ordered CLs of uniform monolayer of dendritic platinum spherical-nanocrowns were engineered by a photo-driven approach. The dendritic platinum nanocrowns were photocatalytically nucleated and autocatalytically grown on each side of photocatalyst-modified membrane. The thickness of the ultra-thin ordered CLs can be controlled to be less than 80 nm and the platinum loading of the CLs on membrane can be varied as low as about 0.01 mg_{Pt}/cm^2each time. The ultra-thin ordered CLs well retained structural order during hot-pressing process and reached a maximum single cell power density of 1.01 ± 0.05 W/cm² at a platinum loading of 53.3 ± 1.5 μg_{Pt} /$cm^2_{cathode}$. Electrochemical and theoretical analysis suggested that the remarkable activity of the ultra-thin ordered CLs may originate from nanostructured spherical-crowns, efficient mass transport, uniform reaction rate, and the optimized anodic humidity. This photo-driven approach may be extended for the fabrication of ultra-thin ordered CLs of other metal and alloys on various substrates for different applications. However, the platinum nanostructures are needed to be further optimized to improve the durability of the ultrathin ordered catalyst layer.

Conflicts of interest

There are no conflicts to declare.

Author contributions

H.L. and Y.S. conceived and designed the experiments. H.L., J.Q., Y.L. and J.L. performed sample characterization and electrochemical studies. H.L., J.Q., T.R., G.L., Q.M., W.S., H.Y. and R.B. performed the portion of work related to fuel cell test and characterizations. Y.W and J.W. performed the numerical simulations. H.L., J.Q. and Y.B.J. accomplished Microscopy studies. S.Z. and Q.H. carried out CSAFM studies. H.L., J.Q., X.W. and G.C. accomplished XRD measurements. H.L. and Y.S. analyzed experimental data and wrote the paper. All authors discussed the results and commented on the manuscript.

Acknowledgements

This study was partially supported by National Key Research & Development Program of China (Gran No. 2019YFB1504501), the Fundamental Research Funds for the Central Universities (Grant Nos. DUT19ZD208 and DUT20ZD208), Science & Technology Innovation Funds of Dalian (Grant No. 2020JJ25CY003), and Special Funds for Guiding Local Scientific and Technological Development by the Central Government (Grant No. 2020JH6/10500021), the National Science Foundation (CBET-1336873) and the U.S. Department of Energy Fuel Cell Technologies Office, (Technical Development Manager: Nancy Garland and Fuel Cells Program Manager: Dimitrios Dimitrios Papageoropoulos).

Notes and references

1 M. K. Debe, *Nature*, 2012, **486**, 43-51.
2 J. Tollefson, *Nature*, 2010, **464**, 1262-1264.
3 L. Chong, J. Wen, J. Kubal, F. G. Sen, J. Zou, J. Greeley, M. Chan, H. Barkholtz, W. Ding and D.-J. Liu, *Science*, 2018, **362**, 1276-1281.
4 G. Shen, J. Liu, H. B. Wu, P. Xu, F. Liu, C. Tongsh, K. Jiao, J. Li, M. Liu, M. Cai, J. P. Lemmon, G. Soloveichik, H. Li, J. Zhu and Y. Lu, *Nat. Commun.*, 2020, **11**, 1191.
5 Y. Zeng, Z. Shao, H. Zhang, Z. Wang, S. Hong, H. Yu and B. Yi, *Nano Energy*, 2017, **34**, 344-355.
6 B. Rod, M. Karren and W. Adam, *https://www.hydrogen.energy.gov/pdfs/review18/fc135_borup_2018_o.pdf*, 2018.
7 O. H. Kim, Y. H. Cho, S. H. Kang, H. Y. Park, M. Kim, J. W. Lim, D. Y. Chung, M. J. Lee, H. Choe and Y. E. Sung, *Nat. Commun.*, 2013, **4**, 2473.
8 A. Kongkanand, N. P. Subramanian, Y. Yu, Z. Liu, H. Igarashi and D. A. Muller, *ACS Catal.*, 2016, **6**, 1578-1583.
9 E. Middelman, *Fuel Cells Bull.*, 2002, **2002**, 9-12.
10 D. F. van der Vliet, C. Wang, D. Tripkovic, D. Strmcnik, X. F. Zhang, M. K. Debe, R. T. Atanasoski, N. M. Markovic and V. R. Stamenkovic, *Nat. Mater.*, 2012, **11**, 1051-1058.
11 Z. Q. Tian, S. H. Lim, C. K. Poh, Z. Tang, Z. Xia, Z. Luo, P. K. Shen, D. Chua, Y. P. Feng, Z. Shen and J. Lin, *Adv. Energy Mater.*, 2011, **1**, 1205-1214.
12 Z. Xia, X. Zhang, H. Sun, S. Wang and G. Sun, *Nano Energy*, 2019, **65**, 104048.
13 W. Zhang, A. I. Minett, M. Gao, J. Zhao, J. M. Razal, G. G. Wallace, T. Romeo and J. Chen, *Adv. Energy Mater.*, 2011, **1**, 671-677.
14 R. Sun, Z. Xia, L. Shang, X. Fu, H. Li, S. Wang and G. Sun, *J. Mater. Chem. A*, 2017, **5**, 15260-15265.

15 Y. Zeng, H. Zhang, Z. Wang, J. Jia, S. Miao, W. Song, Y. Xiao, H. Yu, Z. Shao and B. Yi, *J. Mater. Chem. A*, 2018, **6**, 6521-6533.
16 J. E. Park, S. Kim, O.-H. Kim, C.-Y. Ahn, M.-J. Kim, S. Y. Kang, T. I. Jeon, J.-G. Shim, D. W. Lee, J. H. Lee, Y.-H. Cho and Y.-E. Sung, *Nano Energy*, 2019, **58**, 158-166.
17 C. Pan, H. Wu, C. Wang, B. Wang, L. Zhang, Z. Cheng, P. Hu, W. Pan, Z. Zhou, X. Yang and J. Zhu, *Adv. Mater.*, 2008, **20**, 1644.
18 M. K. Debe, *https://www.hydrogen.energy.gov/pdfs/review09/fc_17_debe.pdf*, 2009.
19 M. K. Debe, *J. Electrochem. Soc.*, 2013, **160**, F522-F534.
20 A. J. Steinbach, *https://www.hydrogen.energy.gov/pdfs/review19/fc143_steinbach_2019_o.pdf*, 2019.
21 K. Schmidt-Rohr and Q. Chen, *Nat. Mater.*, 2008, **7**, 75-83.
22 Y. J. Song, Y. Yang, C. J. Medforth, E. Pereira, A. K. Singh, H. F. Xu, Y. B. Jiang, C. J. Brinker, F. van Swol and J. A. Shelnutt, *J. Am. Chem. Soc.*, 2004, **126**, 635-645.
23 W. Si, J. Li, H. Li, S. Li, J. Yin, H. Xu, X. Guo, T. Zhang and Y. Song, *Nano Res.*, 2013, **6**, 720-725.
24 R. Datta and N. H. Jalani, *J. Electroanal. Chem.*, 2005, **264**, 167-175.
25 Q. Wang, M. Eikerling, D. Song and Z. S. Liu, *J. Electroanal. Chem.*, 2007, **154**, F95-F101.
26 M. K. Debe, *3M/DOE Cooperative Agreement No. DE*, 2007.
27 B. Bladergroen, H. Su, S. Pasupathi and V. Linkov, in *Electrolysis*, eds. V. Linkov and J. Kleperis, 2012, ch. 3.
28 C. H. Park, S. Y. Lee, D. S. Hwang, D. W. Shin, D. H. Cho, K. H. Lee, T. W. Kim, T. W. Kim, M. Lee, D. S. Kim, C. M. Doherty, A. W. Thornton, A. J. Hill, M. D. Guiver and Y. M. Lee, *Nature*, 2016, **532**, 480-483.
29 Y. Wang, *J. Electrochem. Soc.*, 2007, **154**, B1041-B1048.
30 Y. Wang, K. S. Chen, J. Mishler, S. C. Cho and X. C. Adroher, *Appl. Energy*, 2011, **88**, 981-1007.
31 Y. Wang and X. Feng, *J. Electrochem. Soc.*, 2008, **155**, B1289.

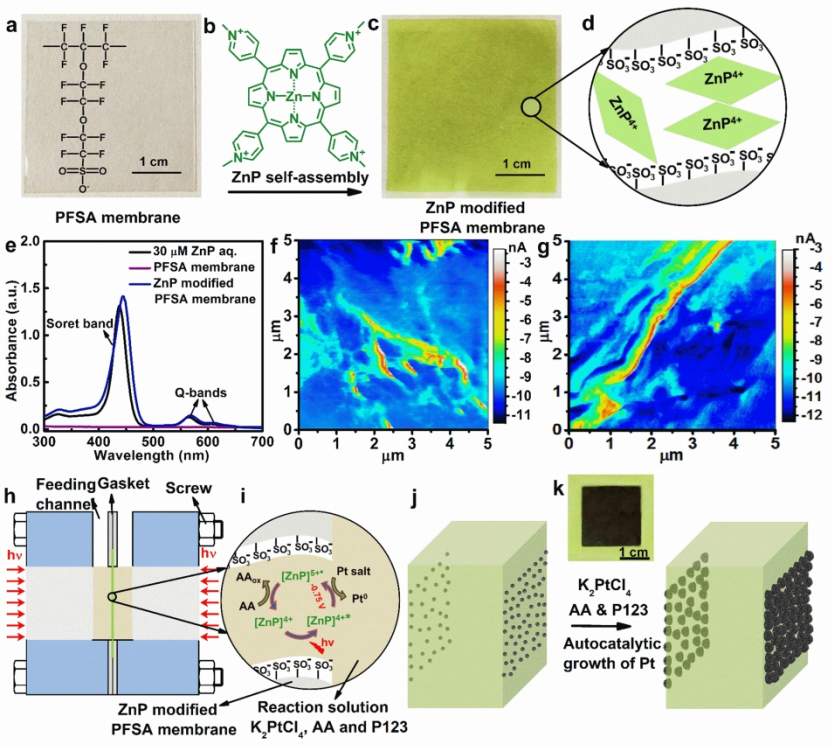

Fig. 1 Nano-engineering of ordered CLs by a photo-driven approach. (a) Photograph and molecular structure of PFSA membrane; (b) molecular structure of ZnP; (c) photograph of a piece of ZnP decorated PFSA membrane; (d) schematic diagram of the distribution of individual ZnP molecules in hydrophilic channels of the membrane; (e) UV-vis spectra of ZnP aq. and the membrane with and without self-assembled ZnP; (f) CSAFM image of pristine membrane; (g) CSAFM image of ZnP decorated membrane; (h) schematic diagram of a bi-square-windowed demountable reactor vertically bisected by the ZnP decorated membrane filled with two separated yellowish reaction mixture; (i) schematic diagram of ZnP based photocatalytic cycle occurring at the interface of membrane and reaction mixture; (j) schematic diagram of autocatalytic growth of platinum seeds into (sub)monolayer of nanostructures on both sides of ZnP decorated membrane, forming a MEA coated with ordered CLs; and (k) a photograph of the MEA with ordered CLs.

272x208mm (300 x 300 DPI)

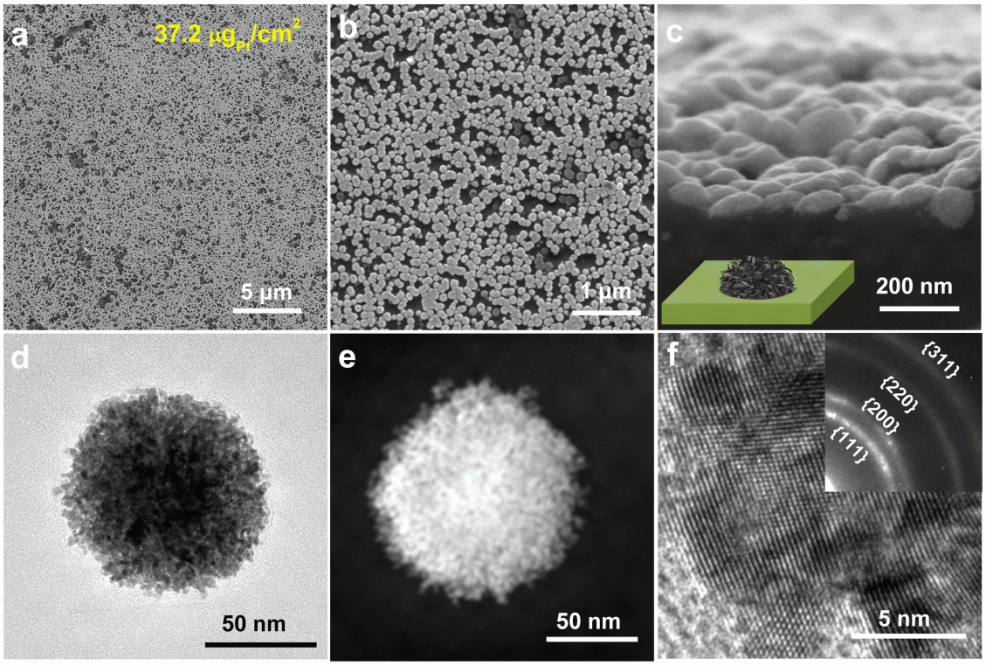

Fig. 2 (a, b) SEM images at different magnifications and (c) SEM image of cross-section view of uniform platinum submonolayer at a loading of 37.2 μgPt/cm2; (d) TEM image, (e) HAADF TEM image, and (f) HRTEM image of a dendritic platinum spherical-nanocrown. Inset: cartoon of a spherical-crown residing on membrane (in (c)) and SAED pattern of a dendritic platinum spherical-nanocrown (in (f)).

272x208mm (300 x 300 DPI)

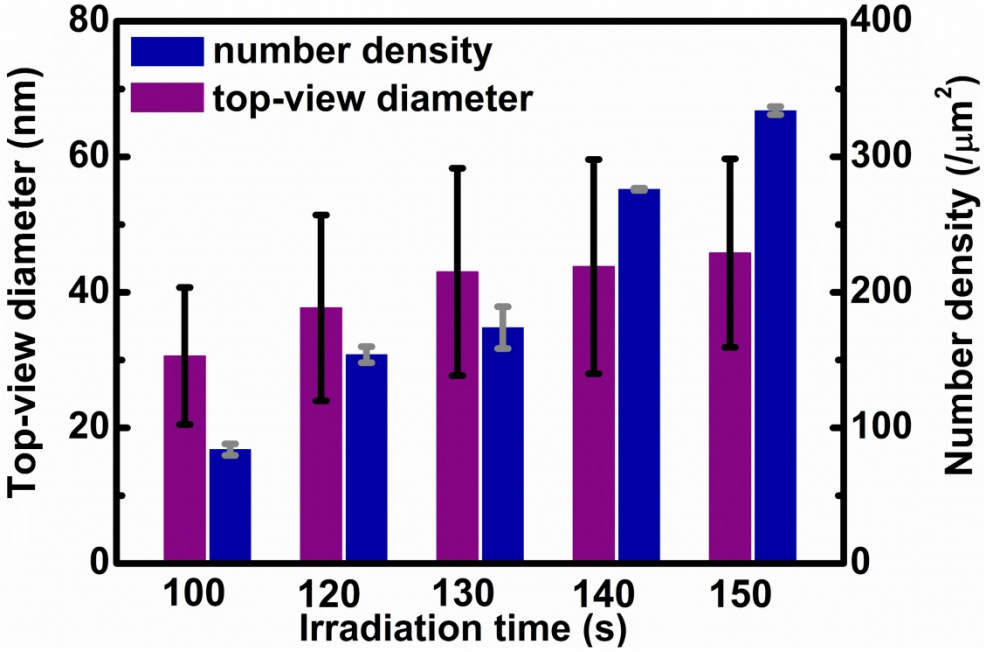

Fig. 3 Change of number density and average top-view diameter of nascent platinum spherical-nanocrowns with irradiation time.

272x208mm (300 x 300 DPI)

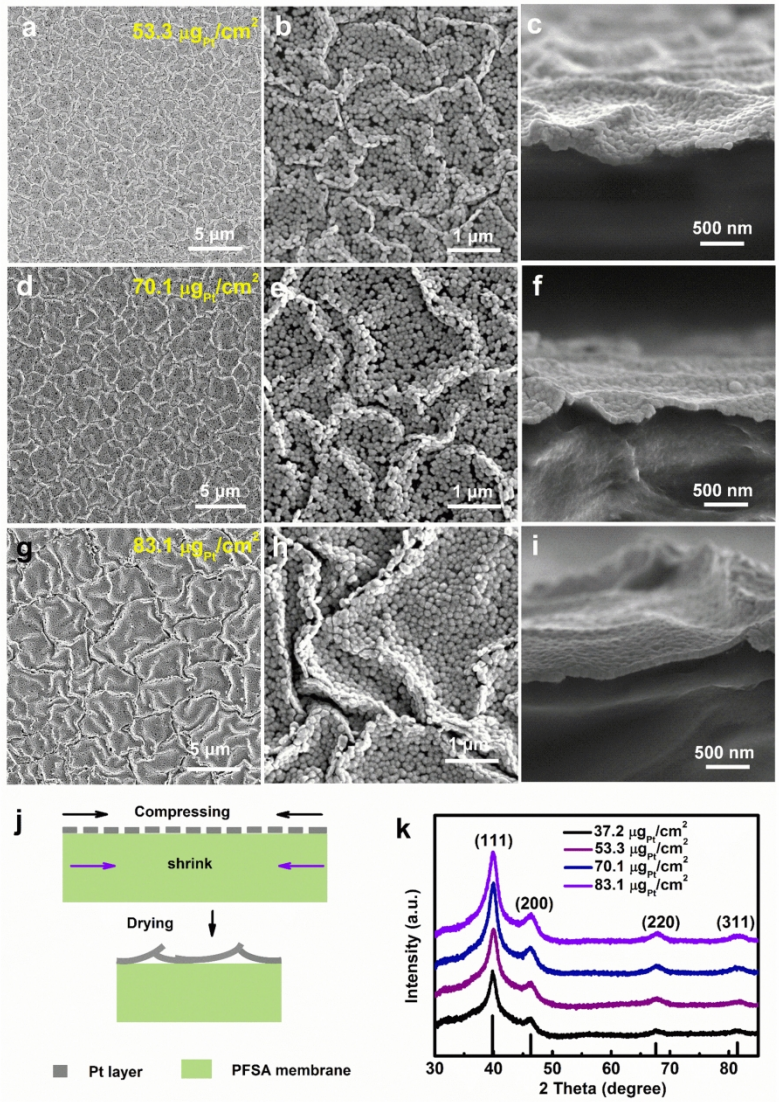

Fig. 4 (a, b) SEM images at different magnifications and (c) SEM image of cross-section view of uniform platinum monolayer at a loading of 53.3 μgPt/cm2; (d, e) SEM images at different magnifications and (f) SEM image of cross-section view of uniform platinum monolayer at a loading of 70.1 μgPt/cm2; (g, h) SEM images at different magnifications and (i) SEM image of cross-section view of uniform platinum monolayer at a loading of 83.1 μgPt/cm2; (j) schematic diagram of platinum layer coated on a membrane before and after drying; (k) XRD patterns of platinum (sub)monolayer single-side coated on membrane at different loadings from 37.2 to 83.1 μgPt/cm2.

219x249mm (300 x 300 DPI)

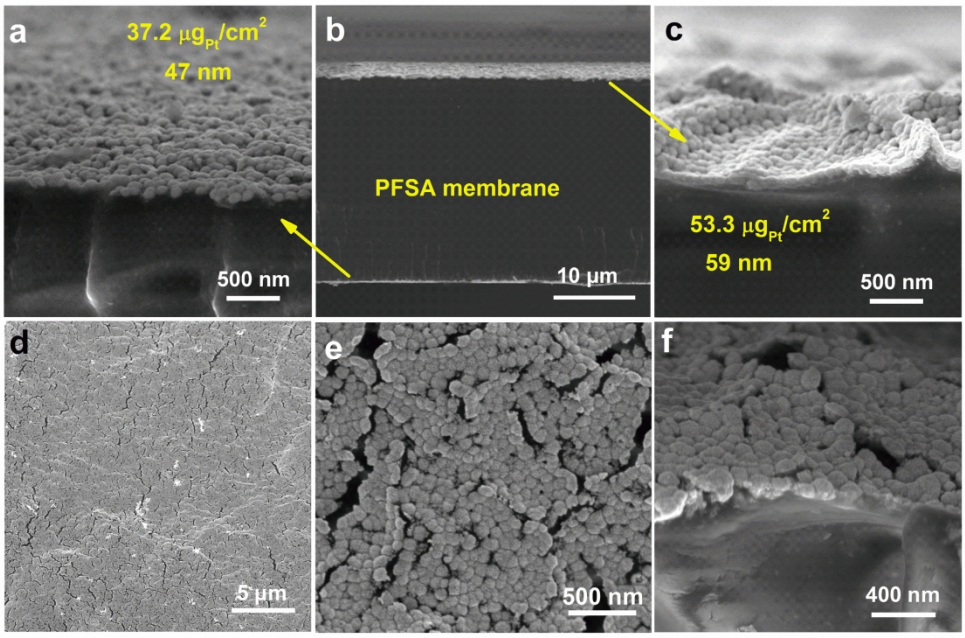

Fig. 5 (a) SEM image of cross-section view of platinum submonolayer uniformly coating one side of membrane with a loading of 37.2 μgPt/cm2; (b) SEM image of cross-section view of a MEA obtained by liquid nitrogen fracturing; (c) SEM image of cross-section view of platinum monolayer uniformly coating the other side of membrane with a loading of 53.3 μgPt/cm2; Top-view SEM images (d, e) and the cross-section view of SEM images (f) of the ordered CL with a loading of 53.3 μgPt/cm2 after being hot-pressed at 125 oC and 6.4 MPa for 2 min.

272x208mm (300 x 300 DPI)

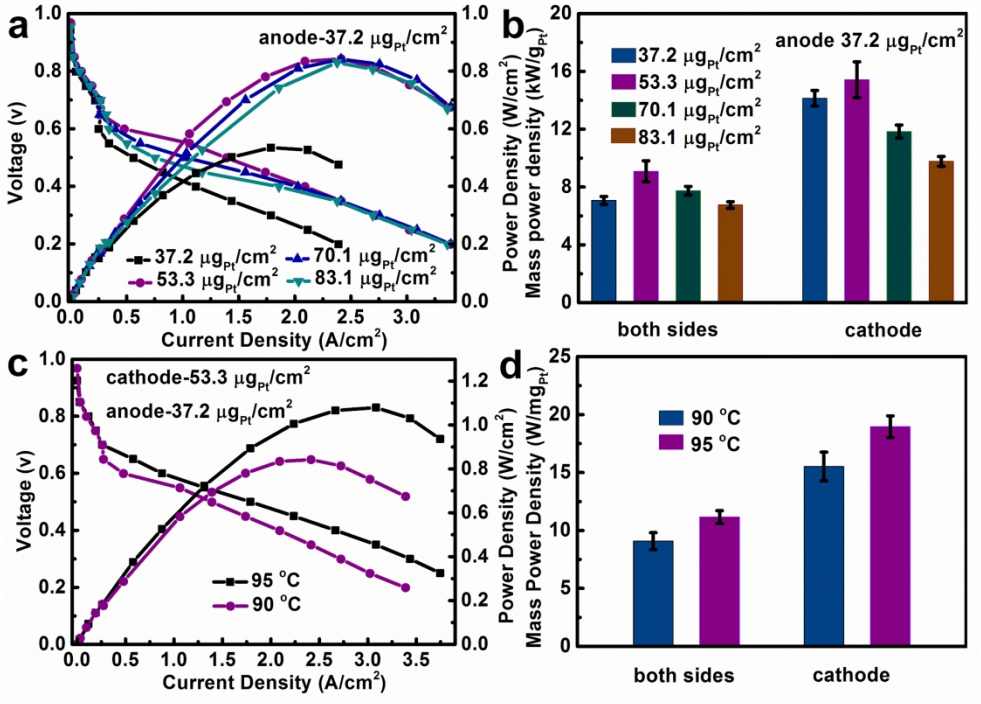

Fig. 6 (a) polarization curves and power density plots and (b) mass specific power density diagram of single cells equipped with the MEAs with cathodic platinum loading varying from 37.2 to 83.1 μg/cm2cathode and constant anodic Pt loading of 37.2 μg/cm2anode (cell at 90 oC, H2 and O2 humidifier at 90 oC, H2/O2 at 100/200 mL/min, back pressure at 0.2 MPagauge for both anode and cathode); (c) polarization curves and power density plots and (d) mass specific power density diagram of single cells equipped with the MEA at cathodic and anodic platinum loading of 53.3 and 37.2 μg/cm2, respectively, and H2 humidifier temperature at 90 and 95 oC (cell at 90 oC, O2 humidifier temperature at 90 oC, H2/O2 at 100/200 mL/min, back pressure at 0.2 MPagauge for both anode and cathode).

272x208mm (300 x 300 DPI)

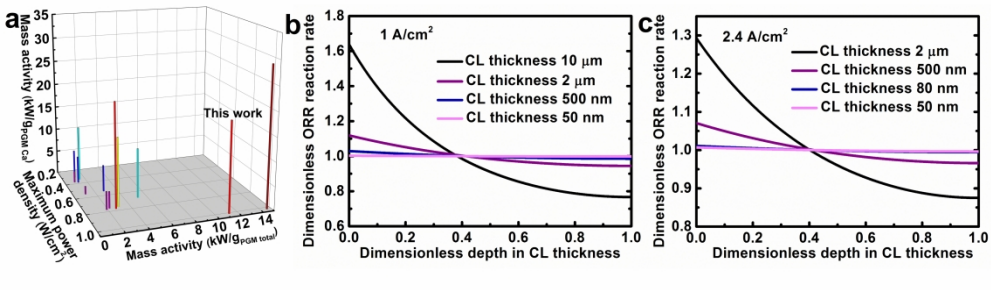

Fig. 7 (a) The maximum power density, mass activity based on total platinum group metal (PGM) loading and PGM loading at only cathode of MEAs with ordered CLs according to Tab. S3; (b) Spatial variation of dimensionless ORR rate across CLs with different thickness at 1 A/cm2; (c) spatial variation of dimensionless ORR rate across CLs with different thickness at 2.4 A/cm2. (Note: The abscissa changes from 0 to 1 means the change from the interface between membrane and CL to the interface between CL and gas diffusion layer.)

405x149mm (300 x 300 DPI)

Graphical Abstract

MEAs with ordered electrocatalyst layers are fabricated by regio-selective growth of monolayer of platinum spherical-nanocrowns on photocatalyst-decorated membrane under irradiation.